Accepted Manuscript

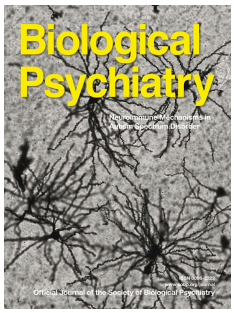

Aberrant Cortical Integration in First-Episode Psychosis During Natural Audiovisual Processing

Teemu Mäntylä, Lauri Nummenmaa, Eva Rikandi, Maija Lindgren, Tuula Kieseppä, Riitta Hari, Jaana Suvisaari, Tuukka T. Raij

PII: S0006-3223(18)31469-0

DOI: 10.1016/j.biopsych.2018.04.014

Reference: BPS 13525

To appear in: *Biological Psychiatry*

Received Date: 15 November 2017

Revised Date: 16 April 2018

Accepted Date: 22 April 2018

Please cite this article as: Mäntylä T., Nummenmaa L., Rikandi E., Lindgren M., Kieseppä T., Hari R., Suvisaari J. & Raij T.T., Aberrant Cortical Integration in First-Episode Psychosis During Natural Audiovisual Processing, *Biological Psychiatry* (2018), doi: 10.1016/j.biopsych.2018.04.014.

TITLE PAGE

Aberrant Cortical Integration in First-Episode Psychosis During Natural Audiovisual Processing

Short form: Aberrant Integration in Psychosis During Movie Viewing

Teemu Mäntylä[1,2,3], Lauri Nummenmaa[2,4], Eva Rikandi[1,2,3], Maija Lindgren[1], Tuula Kieseppä[1,5], Riitta Hari[2,6], Jaana Suvisaari[1] & Tuukka T. Raij[2,5]

[1]*Mental Health Unit, National Institute for Health and Welfare, Helsinki, Finland*

[2]*Department of Neuroscience and Biomedical Engineering, and Advanced Magnetic Imaging Center, Aalto NeuroImaging, Aalto University School of Science, Espoo, Finland*

[3]*Department of Psychology and Logopedics, University of Helsinki, Helsinki, Finland*

[4]*Turku PET Centre and Department of Psychology, University of Turku, Turku, Finland*

[5]*Department of Psychiatry, Helsinki University and Helsinki University Hospital, Helsinki, Finland*

[6]*Department of Art, School of Arts, Design and Architecture, Aalto University, Helsinki, Finland*

Corresponding author: Teemu Mäntylä, Mental Health Unit, National Institute for Health and Welfare, PO Box 30, FI-00271, email: teemu.mantyla@thl.fi

Keywords: first-episode psychosis; intersubject correlation; functional magnetic resonance imaging; disintegration; natural stimulation; default-mode network

Abstract word count: 250

Main text word count: 3990

Figures: 4

Tables: 2

Supplemental information: 1

ABSTRACT

Background: Functional magnetic resonance imaging (fMRI) studies of psychotic disorders have reported both hypo- and hyperactivity in numerous brain regions. In line with the dysconnection hypothesis, these regions include cortical integrative hub regions. However, most earlier studies have focused on a single cognitive function at a time, assessed by delivering artificial stimuli to chronic patients. Thus, it remains unresolved whether these findings are present already in early psychosis and whether they translate to real-life-like conditions which require multisensory processing and integration.

Methods: Fifty-one first-episode psychosis (FEP) patients (16 females) and 32 community-based control subjects (17 females) were shown scenes from Burton's Alice in Wonderland during 3T fMRI. We compared intersubject correlation (ISC), a measure of similarity of brain signal time courses in each voxel, between the groups. We also quantified the hubness as the number of connections each region has.

Results: ISC was significantly lower in FEP patients than in control subjects in the medial and lateral prefrontal, cingulate, precuneal and parietotemporal regions, including the default-mode network. Regional magnitude of between-group difference in ISC was associated with the hubness.

Conclusions: Our findings provide novel evidence for the dysconnection hypothesis by showing that during complex real-life-like stimulus, the most prominent functional brain alterations in psychotic disorders relate to integrative functions. Presence of such abnormalities in FEP rules out long-term effects of illness or medication. These methods can be used in further studies to map widespread hub alterations in a single fMRI session and link them to potential down-stream and up-stream pathways.

TEXT

INTRODUCTION

Schizophrenia and other psychotic disorders have been suggested to result from a compromised integration of neural signals from specialized subsystems in the brain, such as perception, language, memory, and emotions (1–3). In task-related functional magnetic resonance imaging (fMRI) studies, differences between schizophrenia patients and healthy control subjects vary depending on the experimental task (4) with remarkably little regional overlap across tasks (5). A recent meta-analysis suggests, however, that functional changes in chronic schizophrenia patients converge on several “hub” regions, such as the medial and lateral prefrontal cortex, anterior cingulate cortex, thalamus, and the lateral temporal areas (5) that integrate signals from many parts of the brain (6, 7). Whether such an involvement of cortical hub regions occurs already in early psychosis or is simply a consequence of the chronic disorder remains unknown.

There is also no consensus regarding the most pronounced aberrations in brain function that alter the processing of the rich and complex everyday situations in psychotic patients. Studying brain activity of subjects who view a movie provides an excellent assay for investigating such complex processing (8). An audiovisual movie can include sensory, motor, emotional, motivational, social, and cognitive contents in a narrative context. To construct a subjective understanding of the movie, the movie events must be integrated with the individual’s semantic and autobiographical memory, and with the present context (9, 10).

Compared with resting-state fMRI studies (11), where brain activity is recorded without any specific tasks or external stimuli, fMRI recordings during a movie provide the advantage that a significant proportion of the measured brain signals reflects stimulus-driven activity that can be compared between groups and time points. In intersubject correlation (ISC) analysis (12), voxel-

wise functional time series is correlated with the time series of the same voxel in other individuals, providing a measure of how synchronous the brain activity of an individual is with respect to other subjects of the group.

This measure has been used to study patient groups (13–17). For example, in a recent study, ISC was lower during movie viewing in depressive patients compared with a control group in regions important in the regulation of emotions and attention (17). On the other hand, participants diagnosed with Asperger's syndrome showed lower ISC in regions contributing to social information processing (15). Despite the ISC analysis showing promise to reveal diagnostically relevant brain substrates of psychiatric disorders, to our knowledge, only one study with 15 first-episode psychosis (FEP) patients using naturalistic stimuli has been conducted (18).

Disintegration is a central tenet in theories of psychotic disorders (19). In terms of graph theory, measures of centrality estimate how connected a certain region of the brain is to other regions (20). In this approach, highly connected regions are often coined as "hubs" (21). Hubs are involved in higher-order, multisensory processing (21, 22), presumably integrating information from areas with which they are connected (21, 23, 24). Thus, as a measure of hubness and integration of brain areas, we calculate the regional weighted degree centrality across the brain.

In the current study, we used ISC analysis to compare brain activation during movie presentation between patients with FEP and control subjects. As the boundaries between reality and fantasy are distorted in patients with psychotic disorders, the stimulus involved scenes from the movie Alice in Wonderland (2010) containing both realistic and fantasy material. We expected ISC to be lower in patients, especially in brain regions relevant for multimodal, higher-level processing and integration, as determined by the region's hubness, such as the medial parietal and frontal, and

lateral prefrontal regions. Furthermore, we hypothesized such regions to be associated, at least in part, with the fantasy content of the movie.

METHODS AND MATERIALS

This study is a part of the Helsinki Early Psychosis Study from which we have recently published a machine-learning study (25) that focused on transient moment-to-moment changes of brain signals during movie fMRI. Although we here used an almost identical data, the research question and analysis methods are different, as we focus on intersubject correlation between signal time courses during the entire 7-min 20-s movie stimulus.

Participants

The Ethics Committee of the Hospital District of Helsinki and Uusimaa approved the study (diary numbers 257/12/03/03/2009 and 226/13/03/03/2013), and all participants gave a written informed consent before participation. Patient's capacity to give informed consent was assessed by the clinician responsible for the treatment.

We recruited from hospitals and outpatient clinics of the Helsinki University Hospital and the Department of Psychiatry, Helsinki City Health Department 51 FEP patients who were having their first contact with psychiatric care for a psychotic disorder. Psychotic symptoms were evaluated with the Brief Psychiatric Rating Scale – Extended (BPRS-E) (26). The inclusion criterion was scoring ≥4 in either the items for Unusual Thought Content or Hallucinations. Patients with substance-induced psychotic disorder or psychotic disorder due to a general medical condition were excluded. Diagnostic assessment was done on the basis of the Research Version of the Structured Clinical Interview for DSM-IV Axis I Disorders (SCID-I) interview (27) and on a careful review of all medical records by a senior psychiatrist. Current medication use was asked in the interview and confirmed from medical records. The clinical assessment of the patients and control subjects has been previously described in more detail (28).

Thirty-two control subjects of the same age group (18–40 years) were recruited through the Finnish Population Register Centre, excluding subjects who were not eligible for MRI, had a history of psychosis, or a chronic neurological, endocrinological, or cardiovascular disease. FEP patients with epilepsy or structural brain anomalies, or not eligible for MRI were excluded from this analysis. All participants had normal or corrected-to-normal vision.

Acquisition of Functional MRI Data

Due to a scanner update during the study, we acquired fMRI data with two 3-T MRI scanners at Aalto AMI Centre, Aalto NeuroImaging, Aalto University School of Science: first with Signa VH/i (GE Healthcare, Chalfont St Giles, UK) with a 16-channel head coil, and then with Magnetom Skyra (Siemens AG, Erlangen, Germany) with a 32-channel coil. The imaging parameters were the same for both scanners. Whole-brain blood-oxygenation-level-dependent (BOLD-fMRI) signal data were acquired with a gradient-echo-planar sequence (TR 1.8 s; TE 30 ms; flip angle 75°; field of view 24 cm; matrix size 64 x 64; 36 slices with a thickness of 4 mm). Fourteen patients and 11 control subjects were studied with the GE scanner, and 37 patients and 21 control subjects with the Siemens scanner. We included participants from both scanners in the same analysis because multisite fMRI studies have shown that a 10% increase in total sample size will increase statistical power as opposed to using only single-scanner data (29); in our case the 10% increase would mean 6 subjects [(37 + 21) * 0.1 = ~6)]. T1-weighted structural images with $1mm^3$ isotropic voxels and T2-weighted structural images were also acquired, and a clinical neuroradiologist evaluated these scans for brain abnormalities.

The Movie Stimulus

During fMRI, the participants were presented five episodes in sequence from the movie Alice in Wonderland, directed by Tim Burton (total duration 7 min 20 s equalling 245 EPI volumes; Walt Disney Pictures, USA, 2010; dubbed in Finnish). This film is in part animated, but human actors are present in every scene. The scenes show Alice's wedding followed by her trip through a rabbit hole to the Wonderland, and subsequent fantasy events (see (25) for detailed description). The movie was projected onto a semitransparent screen centered in the participant's visual field, and stimulus timing was controlled by Presentation Software (Neurobehavioral Systems Inc., Albany, CA, USA). Sound was conveyed through plastic tubes, which were attached to porous EAR-tip (Etymotic Research Inc., Elk Grove Village, IL, USA) earplugs. To insulate scanner noise, foam pads were placed inside and outside the head coil. The volume of the audio track was adapted according to the participant's subjective preference, ensuring it was loud enough to be clearly audible over scanner noise.

Analysis of ISC Images

Computation of Voxel-Wise ISC

Functional volumes were preprocessed in FSL (http://www.fmrib.ox.ac.uk/fsl/). They were first realigned for movement correction, co-registered with the structural images, normalized to MNI template and smoothed with a Gaussian kernel with 8-mm full width at half maximum (FWHM). After regressing out individual head motion, we used ISC toolbox (30) to compute voxel-wise temporal Pearson correlation between every pair of subjects. To allow between-group comparisons, ISCs were calculated separately for the patient and control groups. This resulted in subject-wise ISC images, where voxel intensities reflect how similar each voxel's time course was in relation to the other subjects in the same group. Similar approach has been used in recent between-group ISC comparisons on Asperger's disorder (15) and depression (17). We calculated the ISCs separately for

participants studied with different scanners. Before the ISC images were entered into group-level analyses, they were smoothed with an 8-mm FWHM kernel to account for inaccuracies in normalization and to enhance comparability between groups and scanners.

Group-Level Analysis

ISC differences between the groups were analyzed using nonparametric two-sample tests with SPM (http://www.fil.ion.ucl.ac.uk/spm/) extension SnPM13 (http://warwick.ac.uk/snpm) and 5000 permutations. We pooled the ISC images from both scanners due to good agreement between different scanners in previous functional imaging studies (31, 32), also using the same two scanners as the ones in this study (33). The results of ISC analyses were thresholded at FWE-corrected voxel-wise $p < 0.05$, and an extent of 20 contiguous voxels. The anatomical locations of statistically significant clusters were identified with Automated Anatomical Labelling (34) as implemented in the XjView toolbox (http://www.alivelearn.net/xjview). As a further characterization of the spatial distribution of ISC differences, we calculated the overlap of the group difference map with resting-state networks of a liberally thresholded 7-network parcellation map of the cerebral cortex (35). This parcellation was chosen because of its availability and popularity as well as big sample size (1000 subjects). The results were visualized using MRIcroGL (http://www.mccauslandcenter.sc.edu/mricrogl/home).

We also extracted signal time courses from 1) the regions that were most strongly synchronized in patients and control subjects during the movie (auditory and visual areas shown in Supplemental Figure S1), and 2) the regions showing the largest group difference (default-mode network (DMN)). Group differences in each time point were studied to find common features of the movie that might contribute to the results. See Supplemental Methods for details.

Rating of Movie Content by an Independent Control Group

Because the separation of reality from fantasy is considered central in psychoses, an independent group of control subjects (n = 17, 10 males and 7 females, mean age 26.5 years) not participating in the fMRI recording rated the moment-to-moment realism of the movie events. Each participant was asked to evaluate, by moving a mouse on a continuous scale, how likely the currently seen events would happen in real life (see http://emotion.utu.fi/softwaredata/). The data were recorded as a value between 0 (very unlikely) and 1 (very likely) every 200 ms and were downsampled to 1 TR to be used in modeling brain activity. This regressor was entered into a general linear model in first-level SPM analysis. Mean optic flow (36) was added as a nuisance covariate to control for visual changes based on the movement of objects in the scene. Resulting contrast images were then compared between groups as well as analyzed as one pooled sample with SnPM to show areas where BOLD signal associated significantly with the fantasy ratings across patients and control subjects. ISC differences were then corrected for multiple comparisons within these areas to show whether fantasy processing-related and ISC difference areas overlap.

Control for Potential Confounders

Attentional differences might account for some group differences in ISC, because attention modulates sensory and cognitive processing (37–42). To control for attentional differences across groups, we computed a map of ISCs in the auditory and visual cortices balanced for scanners and groups (11 subjects included from each group for each scanner, total n = 44). This map was thresholded at pseudo $t > 22$ (for a definition of pseudo t, see e.g. (43)) to include only the brain regions that showed the strongest ISC across participants, i.e. the visual and auditory cortices (Supplemental Figure S1). We then extracted eigenvariates for subject-wise ISCs in this mask. These eigenvariates were entered as a nuisance covariate in a whole-brain ISC group comparison. In addition, age, sex, scanner, mean framewise head movement computed according to Jenkinson et

al. (44), and chlorpromazine (CPZ) daily dose equivalents calculated according to Andreasen et al. (45), except sertindole that was not available in the Andreasen et al. according to (46), were entered as nuisance covariates to exclude potential confounds in the group ISC analyses. As a complementary control for attentional confounds, we report results in the Supplemental Results where the group differences are controlled by extracted ISCs from the dorsal attention network. To further exclude confounding factors, we studied ISC group differences separately for subgroups of patients divided by median framewise displacement, and for the Siemens scanner subgroup (Supplemental Results). We also plotted ISC values to identify outliers that might contribute to findings, and report a complementary ISC analysis less susceptible to outliers (Supplemental Results).

Degree Centrality and ISC Differences

To test whether the ISC differences and the integrative functions of the brain coincide, we computed Pearson's correlation coefficient between the ISC group difference and hubness across voxels. We used the SPM contrast image including all the brain voxels (not only voxels of significant differences) from a two-sample *t* test on ISC differences of control subjects vs patients as a group difference map. The same nuisance covariates were included as in the main analysis. Hubness was measured in control subjects as weighted degree centrality (see e.g. (47)), a measure of the amount of functional connectivity of a voxel across the brain, by using the same BOLD data as in the ISC analysis. Preprocessing for the degree centrality computation included MaxCorr (25, 48) to reduce movement-related artifacts, and the fMRI signals from the cerebrospinal fluid and white matter were extracted and regressed out to restrict potential confounding effects of movement. Weighted degree centrality was then computed in DPARSFA (49) with a default threshold connectivity value of 0.2. SPM second-level one-sample contrast image was computed to represent mean voxel-wise weighted degree among the control subjects. Voxel-wise spatial

correlation between the ISC difference map and the hubness map was calculated within a mask: only voxels in SPM gray-matter template (threshold voxel value = 0.4) and in the map of ISC in control subjects thresholded with FWE-corrected voxel-level $p < 0.001$ were included. The ISC map was used to exclude gray-matter areas with signal loss due to susceptibility artifacts.

RESULTS

Participant Characteristics

Table 1 presents the characteristics of the participants. Patients were on average 1.5 years (median) younger than the control subjects and the patient group included more males (69% vs. 47%). CPZ-equivalent daily dose was on average 365 mg (range 0–1214 mg) in the patients.

ISC Findings

ISC was strongest in both groups in visual and auditory cortices but significantly weaker in patients than in control subjects in the precuneus/posterior cingulate cortex (precuneus/PCC), anterior cingulate cortex/medial prefrontal cortex (ACC/MPFC), bilateral posterior middle temporal gyrus (MTG), angular gyrus, supramarginal gyrus, inferior parietal lobule (the latter four regions called temporo-parietal junction (TPJ) for convenience), middle and inferior frontal gyrus, (called dorso- (DLPFC) and ventrolateral prefrontal cortex (VLPFC), respectively, for convenience), superior frontal gyrus, putamen, cerebellum as well as in the right Heschl's gyrus/posterior insula, thalamus and MTG, left pre- and postcentral gyrus, caudate nucleus, and occipital regions (Figure 1 and Table 2; see Supplemental Table S1 for mean ISC from all clusters for patients and control subjects). These differences remained statistically significant when adjusted for potential confounding effects of the ISCs from visual and auditory cortices (a proxy of attention to the stimulus; see also Supplemental Results, Table S2 and Figure S4 for dorsal attention network-controlled results), age, sex, head movement, scanner and antipsychotic dose equivalents. Compared with the resting-state atlas (35), 40% of the cortical (i.e. excluding subcortical differences) ISC difference map overlapped with the DMN, and the overlap with the other 6 networks was <16% for each (see Figure 2). Note that in this parcellation the somatomotor, auditory and posterior insular cortices are included in the same network (35). Two clusters in posterior

occipital lobe (cluster size (k) = 1.1 cm^3, P = 0.0002, peak at x = −22, y = −94, z = 6; and k = 0.7 cm^3, P = 0.006, peak at x = 10, y = −90, z = −12) showed significantly higher ISC in the patient group than in the control group. However, these differences reached statistical significance only after the inclusion of the ISCs from visual and auditory cortices to the model as a nuisance covariate.

We show in the Supplemental Results that findings were similar in the high-motion (n = 26) and low-motion (n = 25) subgroups (see also Figures S2 and S3). Also, the use of two scanners did not have a major effect as most of the same clusters as in the main analysis showed a significant difference when using only data acquired with the Siemens scanner (Supplemental Results, Figure S5). ISC distributions suggest that the group differences were not driven by only few deviant patients (Supplemental Results; see also Figures S6–S8). Neither the z-scored signals nor the squared differences from the group mean differed statistically significantly between the groups at any time point.

Association with Degree Centrality

Figure 3 presents the overlap between ISC group difference and the weighted degree centrality of the control subjects. The highest degree was found in the precuneus/PCC, ACC/dorsal MPFC, in the lateral occipital, parietal and temporal regions as well as the dorsolateral prefrontal cortex, all of which overlap extensively with areas where between-groups ISC differences were found. Pearson's correlation coefficient r between the ISC group difference (control > patient) and the weighted degree centrality of the control subjects was 0.46, showing that the more functionally connected a region was, the greater the difference in its ISC between the patient and control groups.

Association of BOLD Signal with Fantasy Content of the Stimulus

No group differences were found in a whole-brain analysis of the association between BOLD signal and fantasy content. In a pooled sample of both patients and control subjects, the fantasy content of the movie correlated with BOLD signals of the occipital, temporal and parietal lobes as well as of the dorsolateral prefrontal cortices (Figure 4). These regions overlapped with the ISC group difference in bilateral precuneus/PCC, TPJ, precentral, and VLPFC, and in right DLPFC, Heschl's gyrus/posterior insula and MTG.

DISCUSSION

We found significantly weaker ISC during movie viewing in FEP patients than in control subjects in widespread brain regions, including precuneus/PCC, ACC/MPFC, TPJs, lateral prefrontal cortices, higher-level occipital areas, and right MTG, as well as in subcortical structures. The differences between patients and control subjects remained statistically significant even after adjusting for ISCs in the visual and auditory sensory areas, which suggests the group differences are not due to different input to primary sensory areas, or due to compromised attention in the patients. Although the significant clusters in the right MTG and posterior insula/Heschl's gyrus coincided with early auditory cortical areas, the MTG cluster extended to association cortical areas and largely overlapped with lateral temporal regions of the DMN.

Mapping disorder-related brain activity alterations that are relevant to processing of natural, dynamic and multimodal stimuli helps to understand how the pathogenesis of psychotic disorders contributes to everyday sensory, cognitive, and affective processing. While numerous task-selective functional brain alterations have been reported in FEP patients, they may not directly translate to brain function during everyday life (50). Natural and dynamic stimuli consistently trigger more reproducible brain activity than do highly specific stimuli (51), especially in higher-level regions, and brain regions showing no net activity changes to repeated stimuli might still respond reliably to complex stimuli (52).

Several of these regions, such as the precuneus/PCC, ACC/MPFC, TPJs and lateral prefrontal cortices (22, 47), are considered as high-level areas integrating signals from multiple brain systems. Although altered low-level sensory processing might contribute to psychotic symptoms (53, 54), the main deficits in psychosis patients seem thus to result from disintegrated higher-level functions,

preventing coherent, dynamic perceptions, and the adaptive interaction of cognition and emotions and their appropriate contextualisation through memory (2, 55). The hubness, measured in control subjects, was correlated with the magnitude of ISC group differences, suggesting that the largest ISC differences predominate in hub regions. Accordingly, the current ISC differences overlapped with cortical hubs as defined in previous studies (21, 22). Structural and resting-state functional imaging have shown psychosis-related alterations both in the hubs and in whole-brain network topology supporting global integration. Such alterations have been reported in FEP patients (56), chronic schizophrenia patients (57–59), their unaffected siblings (60), and in population-based samples of people with sub-clinical psychotic experiences (61). A pooled analysis on task-fMRI studies in chronic schizophrenia patients has shown overrepresentation of functional alterations in hubs compared with non-hub regions (5). Our findings imply that the prominence of hub alterations can be quantified during a single fMRI session, instead of using a set of multiple simple tasks (5), by employing a naturalistic movie stimulus.

Many regions where we observed ISC differences, including the precuneus/PCC, ACC/MPFC and TPJs, overlap with the DMN (35, 62–64). In our earlier machine-learning analysis using the same cohort, moment-to-moment changes in the BOLD signal differentiated patients and control subjects with an average 77.5% accuracy, based largely on the functioning of the precuneus/PCC (25). Accordingly, the statistically most significant ISC differences between the groups occurred in the central hub region of the DMN—the precuneus/PCC. DMN has been proposed to serve as a global integrator for conscious experience (65) and to be at the top end of cortical connectivity hierarchy (66). The precuneus/PCC, ACC/MPFC and TPJs have longer temporal receptive windows than lower-level sensory areas, as evidenced by ISC analysis (67, 68), and may integrate information over minutes (69). In agreement, ISC of these regions may differentiate FEP patients and control subjects better than processing at the word- or sentence-levels (18). In the present study, the activity

in the precuneus/PCC and TPJ regions increased as a function of fantasy content of the movie, together with the activity of the auditory and visual cortices. Notably the sense of reality entails comparing current sensory information with an internal model of the world based on semantic and autobiographical memory, which are related to DMN functioning (9, 70).

The clustering of functional alterations to psychosis patients' hub regions might be related to hubs' high metabolic demands (71, 72). Hub regions integrate signals from several brain networks (73) so that multiple dysfunctions across the brain could converge to them. In general, hub dysfunction might comprise a common denominator of psychotic disorders that can be contributed by heterogeneous lower-level alterations.

Limitations

Patients and control subjects differed in mean age and sex ratio, but controlling for these potential confounders statistically did not alter the main results. Considering the complexity of the movie stimulus, it remains difficult to control for all the variables that may have contributed to the ISC findings. It could also be speculated that another kind of movie might have resulted in different findings and that some important elements for understanding the brain basis of psychosis may have been missing from the present stimulus, but different kinds of engaging movies tend to elicit ISC in similar areas (51). In agreement, none of the individual time points of the extracted DMN signal separated the groups in the present study.

Conclusions

The most prominent functional brain alterations in FEP patients, observed while the patients were viewing a complex audiovisual movie stimulus, were located in hub regions that subserve integrative brain functions. The diffuse brain alterations shown in previous single-task-fMRI studies

on psychotic disorders might converge on the dysfunction of the integrative hubs during processing of complex real-life-like information. Present methods should be used in further studies to access both up-stream and down-stream pathways of hub dysfunction.

ACKNOWLEDGEMENTS

This work was supported by the Sigrid Jusélius Foundation (J.S.), the Finnish Cultural Foundation (T.M., J.S., and R.H.), the European Research Council (Advanced Grant #232946 to R.H.), the Jalmari and Rauha Ahokas Foundation (T.M.), the Doctoral Program Brain and Mind of the University of Helsinki (T.M.), the Academy of Finland (MIND program grant #265917 to L.N. and grant #278171 to J.S.), the Finnish Medical Foundation (T.T.R.), the Louis-Jeantét Foundation (R.H.), the Yrjö Jahnsson Foundation (#6781 to M.L.), the Päivikki and Sakari Sohlberg Foundation (M.L.), State funding for university-level health research (Hospital District of Helsinki and Uusimaa #TYH2013332, #TYH2014228, #TYH2017128 to T.K.), and the European Union's Seventh Framework Programme for project METSY (# 602478 to J.S.).

We are thankful to all the participants. Tuula Mononen and Sanna Järvinen coordinated the data collection and interviews, Marjut Grainger managed the data and Marita Kattelus assisted in the imaging. We thank Enrico Glerean for providing us with data-collection software for the movie ratings and Juho Kettunen for calculating the optic flow. The movie was presented with permission from the Finnish licence holder (M&M Viihdepalvelu Oy, Vantaa, Finland). Part of these data have been presented in the 5th biennial Schizophrenia International Research Society Conference (Florence, 2016) and the 2nd annual Finnish Symposium on Biological Psychiatry (Helsinki, 2016).

FINANCIAL DISCLOSURES

M.L. has received financial compensation for an interview from Lundbeck. T.K. has got rewards for lectures from Oy H. Lundbeck Ab / Otsuka Pharma Scandinavia AB and Janssen-Cilag Oy.

The other authors report no biomedical financial disclosures or potential conflicts of interest.

REFERENCES

1. Friston KJ (1998): The disconnection hypothesis. *Schizophr Res* 30:115–125.

2. Rubinov M, Bullmore E (2013): Schizophrenia and abnormal brain network hubs. *Dialogues Clin Neurosci* 15:339–349.

3. Stephan KE, Friston KJ, Frith CD (2009): Dysconnection in schizophrenia: From abnormal synaptic plasticity to failures of self-monitoring. *Schizophr Bull* 35:509–527.

4. Goghari VM, Sponheim SR, MacDonald III AW (2010): The functional neuroanatomy of symptom dimensions in schizophrenia: A qualitative and quantitative review of a persistent question. *Neurosci Biobehav Rev* 34:468–486.

5. Crossley NA, Mechelli A, Ginestet C, Rubinov M, Bullmore ET, McGuire P (2016): Altered hub functioning and compensatory activations in the connectome: A meta-analysis of functional neuroimaging studies in schizophrenia. *Schizophr Bull* 42:434–442.

6. Bertolero MA, Yeo BTT, D'Esposito M (2015): The modular and integrative functional architecture of the human brain. *Proc Natl Acad Sci U S A* 112:E6798–E6807.

7. Crossley NA, Mechelli A, Vértes PE, Winton-Brown TT, Patel AX, Ginestet CE, et al (2013): Cognitive relevance of the community structure of the human brain functional coactivation network. *Proc Natl Acad Sci U S A* 110:11583–11588.

8. Hasson U, Honey CJ (2012): Future trends in neuroimaging: Neural processes as expressed within real-life contexts. *Neuroimage* 62:1272–1278.

9. Binder JR, Desai RH, Graves WW, Conant LL (2009): Where is the semantic system? A critical review and meta-analysis of 120 functional neuroimaging studies. *Cereb Cortex* 19:2767–2796.

10. Hasson U, Chen J, Honey CJ (2015): Hierarchical process memory: Memory as an integral component of information processing. *Trends Cogn Sci* 19:304–313.

11. Damoiseaux JS, Rombouts SARB, Barkhof F, Scheltens P, Stam CJ, Smith SM, et al (2006): Consistent resting-state networks across healthy subjects. *Proc Natl Acad Sci U S A* 103:13848–13853.

12. Hasson U, Nir Y, Levy I, Fuhrmann G, Malach R (2004): Intersubject synchronization of cortical activity during natural vision. *Science* 303:1634–1640.

13. Byrge L, Dubois J, Tyszka JM, Adolphs R, Kennedy DP (2015): Idiosyncratic brain activation patterns are associated with poor social comprehension in autism. *J Neurosci* 35:5837–5850.

14. Hasson U, Avidan G, Gelbard H, Vallines I, Harel M, Minshew N, et al (2009): Shared and idiosyncratic cortical activation patterns in autism revealed under continuous real-life viewing conditions. *Autism Res* 2:220–231.

15. Salmi J, Roine U, Glerean E, Lahnakoski J, Nieminen-von Wendt T, Tani P, et al (2013): The brains of high functioning autistic individuals do not synchronize with those of others. *Neuroimage Clin* 3:489–497.

16. Anderson JS, Nielsen JA, Ferguson MA, Burback MC, Cox ET, Dai L, et al (2013): Abnormal brain synchrony in Down Syndrome. *Neuroimage Clin* 2:703–715.

17. Guo CC, Nguyen VT, Hyett MP, Parker GB, Breakspear MJ (2015): Out-of-sync: Disrupted neural activity in emotional circuitry during film viewing in melancholic depression. *Sci Rep* 5:11605.

18. Lerner Y, Bleich-Cohen M, Solnik-Knirsh S, Yogev-Seligmann G, Eisenstein T, Madah W, et al (2018): Abnormal neural hierarchy in processing of verbal information in patients with schizophrenia. *Neuroimage Clin* 17:1047–1060.

19. van den Heuvel MP, Fornito A (2014): Brain networks in schizophrenia. *Neuropsychol Rev* 24:32–48.

20. Bullmore E, Sporns O (2009): Complex brain networks: Graph theoretical analysis of structural and functional systems. *Nat Rev Neurosci* 10:186–198.

21. van den Heuvel MP, Sporns O (2013): Network hubs in the human brain. *Trends Cogn Sci* 17:683–696.

22. Sepulcre J, Sabuncu MR, Yeo TB, Liu H, Johnson KA (2012): Stepwise connectivity of the modal cortex reveals the multimodal organization of the human brain. *J Neurosci* 32:10649–10661.

23. Zamora-López G, Zhou C, Kurths J (2010): Cortical hubs form a module for multisensory integration on top of the hierarchy of cortical networks. *Front Neuroinform* 4:1.

24. van den Heuvel MP, Sporns O (2013): An anatomical substrate for integration among functional networks in human cortex. *J Neurosci* 33:14489–14500.

25. Rikandi E, Pamilo S, Mäntylä T, Suvisaari J, Kieseppä T, Hari R, et al (2017): Precuneus functioning differentiates first-episode psychosis patients during the fantasy movie Alice in Wonderland. *Psychol Med* 47:495–506.

26. Ventura J, Lukoff D, Nuechterlein KH, Liberman RP, Green MF, Shaner A (1993): Appendix 1: Brief Psychiatric Rating Scale (BPRS) Expanded version (4.0) scales, anchor points and administration manual. *Int J Methods Psychiatr Res* 3:227–244.

27. First MB, Spitzer RL, Gibbon M, Williams JBW (2007): *Structured Clinical Interview for DSM-IV-TR Axis I Disorders, Research Version, Patient Edition. (SCID-I/P)*, New York: Biometrics Research, New York State Psychiatric Institute.

28. Mäntylä T, Mantere O, Raij TT, Kieseppä T, Laitinen H, Leiviskä J, et al (2015): Altered activation of innate immunity associates with white matter volume and diffusion in first-episode psychosis. *PLoS One* 10:e0125112.

29. Suckling J, Ohlssen D, Andrew C, Johnson G, Williams SCR, Graves M, et al (2008): Components of variance in a multicentre functional MRI study and implications for calculation of statistical power. *Hum Brain Mapp* 29:1111–1122.

30. Kauppi J, Jääskeläinen IP, Sams M, Tohka J (2010): Inter-subject correlation of brain hemodynamic responses during watching a movie: Localization in space and frequency. *Front Neuroinform* 4:5.

31. Forsyth JK, McEwen SC, Gee DG, Bearden CE, Addington J, Goodyear B, et al (2014): Reliability of functional magnetic resonance imaging activation during working memory in a multi-site study: Analysis from the North American Prodrome Longitudinal Study. *Neuroimage* 97:41–52.

32. Gee DG, McEwen SC, Forsyth JK, Haut KM, Bearden CE, Addington J, et al (2015): Reliability of an fMRI paradigm for emotional processing in a multisite longitudinal study. *Hum Brain Mapp* 36:2558–2579.

33. Raij TT, Mäntylä T, Mantere O, Kieseppä T, Suvisaari J (2016): Cortical salience network activation precedes the development of delusion severity. *Psychol Med* 46:2741–2748.

34. Tzourio-Mazoyer N, Landeau B, Papathanassiou D, Crivello F, Etard O, Delcroix N, et al (2002): Automated anatomical labeling of activations in SPM using a macroscopic anatomical parcellation of the MNI MRI single-subject brain. *Neuroimage* 15:273–289.

35. Yeo BTT, Krienen FM, Sepulcre J, Sabuncu MR, Lashkari D, Hollinshead M, et al (2011): The organization of the human cerebral cortex estimated by intrinsic functional connectivity. *J Neurophysiol* 106:1125–1165.

36. Viinikainen M, Glerean E, Jääskeläinen IP, Kettunen J, Sams M, Nummenmaa L (2012): Nonlinear neural representation of emotional feelings elicited by dynamic naturalistic stimulation. *Open J Neurosci* 2:4.

37. van Kerkoerle T, Self MW, Roelfsema PR (2017): Layer-specificity in the effects of attention and working memory on activity in primary visual cortex. *Nat Commun* 8:13804.

38. Petkov CI, Kang X, Alho K, Bertrand O, Yund EW, Woods DL (2004): Attentional modulation of human auditory cortex. *Nat Neurosci* 7:658–663.

39. Jäncke L, Mirzazade S, Joni Shah N (1999): Attention modulates activity in the primary and the secondary auditory cortex: a functional magnetic resonance imaging study in human subjects. *Neuroscience Letters* 266:125–128.

40. Treue S (2001): Neural correlates of attention in primate visual cortex. *Trends in Neurosciences* 24:295–300.

41. Posner MI, Gilbert CD (1999): Attention and primary visual cortex. *Proc Natl Acad Sci U S A* 96:2585–2587.

42. Poghosyan V, Ioannides AA (2008): Attention Modulates Earliest Responses in the Primary Auditory and Visual Cortices. *Neuron* 58:802–813.

43. Nichols TE, Holmes AP (2002): Nonparametric permutation tests for functional neuroimaging: A primer with examples. *Hum Brain Mapp* 15:1–25.

44. Jenkinson M, Bannister P, Brady M, Smith S (2002): Improved optimization for the robust and accurate linear registration and motion correction of brain images. *Neuroimage* 17:825–841.

45. Andreasen NC, Pressler M, Nopoulos P, Miller D, Ho B (2010): Antipsychotic dose equivalents and dose-years: A standardized method for comparing exposure to different drugs. *Biol Psychiatry* 67:255–262.

46. Haukka J, Suvisaari J, Tuulio-Henriksson A, Lönnqvist J (2007): High concordance between self-reported medication and official prescription database information. *Eur J Pharmacol* 63:1069–1074.

47. Buckner RL, Sepulcre J, Talukdar T, Krienen FM, Liu H, Hedden T, et al (2009): Cortical hubs revealed by intrinsic functional connectivity: Mapping, assessment of stability, and relation to Alzheimer's disease. *J Neurosci* 29:1860–1873.

48. Pamilo S, Malinen S, Hotta J, Seppä M (2015): A correlation-based method for extracting subject-specific components and artifacts from group-fMRI data. *Eur J Neurosci* 42:2726–2741.

49. Yan C, Zang Y (2010): DPARSF: A MATLAB toolbox for pipeline data analysis of resting-state fMRI. *Front Syst Neurosci* 4:13.

50. Adolphs R, Nummenmaa L, Todorov A, Haxby JV (2016): Data-driven approaches in the investigation of social perception. *Philos Trans R Soc Lond B Biol Sci* 371:20150367.

51. Hasson U, Malach R, Heeger DJ (2010): Reliability of cortical activity during natural stimulation. *Trends Cogn Sci* 14:40–48.

52. Ben-Yakov A, Honey CJ, Lerner Y, Hasson U (2012): Loss of reliable temporal structure in event-related averaging of naturalistic stimuli. *Neuroimage* 63:501–506.

53. Uhlhaas PJ, Singer W (2010): Abnormal neural oscillations and synchrony in schizophrenia. *Nat Rev Neurosci* 11:100–113.

54. Javitt DC, Freedman R (2015): Sensory processing dysfunction in the personal experience and neuronal machinery of schizophrenia. *Am J Psychiatry* 172:17–31.

55. Anticevic A, Corlett PR (2012): Cognition-emotion dysinteraction in schizophrenia. *Front Psychol* 3:392.

56. Zhang R, Wei Q, Kang Z, Zalesky A, Li M, Xu Y, et al (2015): Disrupted brain anatomical connectivity in medication-naïve patients with first-episode schizophrenia. *Brain Struct Funct* 220:1145–1159.

57. van den Heuvel MP, Mandl RCW, Stam CJ, Kahn RS, Hulshoff Pol HE (2010): Aberrant frontal and temporal complex network structure in schizophrenia: A graph theoretical analysis. *J Neurosci* 30:15915–15926.

58. Lynall M, Bassett DS, Kerwin R, McKenna PJ, Kitzbichler M, Muller U, et al (2010): Functional connectivity and brain networks in schizophrenia. *J Neurosci* 30:9477–9487.

59. Cheng H, Newman S, Goñi J, Kent JS, Howell J, Bolbecker A, et al (2015): Nodal centrality of functional network in the differentiation of schizophrenia. *Schizophr Res* 168:345–352.

60. Collin G, Kahn RS, de Reus MA, Cahn W, van den Heuvel MP (2014): Impaired rich club connectivity in unaffected siblings of schizophrenia patients. *Schizophr Bull* 40:438–448.

61. Drakesmith M, Caeyenberghs K, Dutt A, Zammit S, Evans CJ, Reichenberg A, et al (2015): Schizophrenia-like topological changes in the structural connectome of individuals with subclinical psychotic experiences. *Hum Brain Mapp* 36:2629–2643.

62. Buckner RL, Andrews-Hanna JR, Schacter DL (2008): The brain's default network. *Ann N Y Acad Sci* 1124:1–38.

63. Zhang S, Li CR (2012): Functional connectivity mapping of the human precuneus by resting state fMRI. *Neuroimage* 59:3548–3562.

64. Raichle ME (2015): The brain's default mode network. *Annu Rev Neurosci* 38:433–447.

65. Vatansever D, Menon DK, Manktelow AE, Sahakian BJ, Stamatakis EA (2015): Default mode dynamics for global functional integration. *J Neurosci* 35:15254–15262.

66. Margulies DS, Ghosh SS, Goulas A, Falkiewicz M, Huntenburg JM, Langs G, et al (2016): Situating the default-mode network along a principal gradient of macroscale cortical organization. *Proc Natl Acad Sci U S A* 113:12574–12579.

67. Hasson U, Yang E, Vallines I, Heeger DJ, Rubin N (2008): A hierarchy of temporal receptive windows in human cortex. *J Neurosci* 28:2539–2550.

68. Lerner Y, Honey CJ, Silbert LJ, Hasson U (2011): Topographic mapping of a hierarchy of temporal receptive windows using a narrated story. *J Neurosci* 31:2906–2915.

69. Simony E, Honey CJ, Chen J, Lositsky O, Yeshurun Y, Wiesel A, et al (2016): Dynamic reconfiguration of the default mode network during narrative comprehension. *Nat Commun* 7:12141.

70. Ames DL, Honey CJ, Chow MA, Todorov A, Hasson U (2015): Contextual alignment of cognitive and neural dynamics. *J Cogn Neurosci* 27:655–664.

71. Liang X, Zou Q, He Y, Yang Y (2013): Coupling of functional connectivity and regional cerebral blood flow reveals a physiological basis for network hubs of the human brain. *Proc Natl Acad Sci U S A* 110:1929–1934.

72. Tomasi D, Wang G, Volkow ND (2013): Energetic cost of brain functional connectivity. *Proc Natl Acad Sci U S A* 110:13642–13647.

73. Leech R, Braga R, Sharp DJ (2012): Echoes of the brain within the posterior cingulate cortex. *J Neurosci* 32:215–222.

74. American Psychiatric Association (2000): *Diagnostic and Statistical Manual of Mental Disorders,* 4th (text rev.) ed. Washington, DC: American Psychiatric Press.

75. Hilsenroth MJ, Ackerman SJ, Blagys MD, Baumann BD, Baity MR, Smith SR, et al (2000): Reliability and validity of DSM-IV Axis V. *Am J Psychiatry* 157:1858–1863.

76. Andreasen NC (1982): Negative symptoms in schizophrenia: definition and reliability. *Arch Gen Psychiatry* 39:784.

FIGURE LEGENDS

Figure 1. Differences in ISC strength, adjusted for nuisance variables (see main text), between control and FEP groups. Significantly ($p < 0.05$, voxel-level FWE-corrected) stronger ISC in control group is displayed; the color bar indicates pseudo *t* value (for pseudo *t*, see (43)). In the transversal slices, left hemisphere is up and in the coronal slice, left is left. ACC/MPFC, anterior cingulate cortex/medial prefrontal cortex; DLPFC, dorsolateral prefrontal cortex; LTPJ, left temporo-parietal junction; MTG, middle temporal gyrus; PC/PCC, precuneus/posterior cingulate cortex; RTPJ, right temporo-parietal junction; VLPFC, ventrolateral prefrontal cortex.

Figure 2. (A) The percentage of ISC difference map that overlaps with particular resting-state network from Yeo et al. (35). **(B)** Selected slices from the resting-state atlas.

Figure 3. Overlap between degree centrality in control subjects (cool colors) and ISC difference map from the main analysis (warm colors). Overlap is shown in green. The maps are thresholded at $t > 8$ and pseudo $t > 3$, respectively, for visualization. The color bars indicate the respective statistical values. In the transversal slice, left hemisphere is up and in the coronal slice, left is left.

Figure 4. Association between online rating of the fantasy content of the movie and BOLD signal in a pooled sample of patients and control subjects (cool colors). The ISC difference is shown (warm colors) for reference (statistical image threshold is voxel-level FWE-corrected $p < 0.05$). The color bars indicate the respective pseudo *t* values.

Table 1. Participant characteristics

	FEP group *n* (%) or median and 1st–3rd quartiles	Control group *n* (%) or median and 1st–3rd quartiles	Test statistic	*P* value
Sex (female)	16/51 (31%)	17/32 (53%)	χ^2 = 3.88	**0.049**
Age (yrs)	23.2 (20.9–27.8)	24.7 (23.0–33.8)	*U* = 593	**0.037**
Head motion (mm)	0.53 (0.37–0.76)	0.56 (0.31–0.64)	*U* = 789	0.801
GAF	35 (31–40)	90 (81.3–90)	*U* = 4.5	**<0.001**
Positive symptoms	7 (3–10)	0	*U* = 112	**<0.001**
Negative symptoms	5 (3–10)	0	*U* = 121	**<0.001**
Diagnosis				
Schizophrenia	23 (45.1%)			
Schizophreniform disorder	10 (19.6%)			
Schizoaffective disorder	1 (2.0%)			
MDD with psychotic features	1 (2.0%)			
Bipolar I disorder, with psychotic features	4 (7.8%)			

Brief psychotic disorder	1 (2.0%)
Psychotic disorder NOS	11 (21.6%)

Statistically significant differences are bolded. FEP, first-episode psychosis; GAF, Global Assessment of Functioning (74, 75); MDD, major depressive disorder; NOS, not otherwise specified. Positive symptoms is the sum score from BPRS (26) items Hallucination, Unusual thought content, Bizarre behaviour and Conceptual disorganization and negative symptoms BPRS item Blunted affect, and alogia, anhedonia-asociality and avolition-apathy from the Scale for the Assessment of Negative Symptoms (SANS) (76). The BPRS item scores were scaled to 0–6 before calculating the sum score.

Table 2. Group comparison of ISCs. Table shows where ISCs are higher in control subjects.

Region	Peak (MNI) x, y, z	Minimum *p* value[a]	Extent (cm^3)
Parietal, temporal, occipital			
Bilateral precuneus, cuneus, PCC, pMCC, and calcarine cortex	12, −64, 24	0.0002	42.9
Right MTG (incl. STG & ITG)	52, −30, −4	0.0002	4.2
Left TPJ, incl. MOG	−48, −76, 14	0.0002	13.2
Right TPJ	50, −48, 20	0.0002	8.7
Left calcarine and lingual gyri	−24, −66, 4	0.0004	0.7
Right posterior insula and Heschl's gyrus	38, −20, 12	0.0046	0.7
Right fusiform gyrus	34, −38, −20	0.0074	0.2
Right MOG	36, −78, 20	0.0078	0.6
Left MOG	−34, −82, 28	0.0012	1.9
Frontal			
Left DLPFC	−28, 46, 18	0.0002	6.0
Left VLPFC, incl. STP	−48, 32, −12	0.0002	4.5
Right aVLPFC, incl. STP	48, 22, −16	0.0002	2.7
Right pVLPFC	46, 22, 14	0.0002	1.5
Bilateral ACC, aMCC and MPFC	0, 16, 32	0.0004	5.4
Left pre- and postcentral gyrus	−52, −6, 48	0.0010	1.0
Right DLPFC	26, 54, 20	0.0010	6.9
Right orbitofrontal cortex	44, 48, −12	0.0010	1.2
Left aSFG and medial SFG	−14, 60, 24	0.0010	0.4
Right SMA and medial SFG	8, 24, 60	0.0034	0.6
Left pSFG and medial SFG	−10, 34, 52	0.0038	0.6
Left SMA	−8, 10, 66	0.0044	0.8
Right (posterior) MFG and precentral gyrus	34, −2, 52	0.0078	0.6
Subcortical			
Left cerebellum (8)	−28, −62, −60	0.0002	0.6
Bilateral cerebellum (9 & Vermis 9)	6, −56, −46	0.0002	1.4
Right cerebellum (7b, 8 & Vermis 8)	4, −74, −44	0.0002	0.9
Right cerebellum (8 & 10)	32, −40, −46	0.0002	0.4
Left putamen	−20, 4, −10	0.0010	0.6
Left cerebellum (Crus 2 & 7b)	−22, −82, −44	0.0012	1.1
Right cerebellum (8)	26, −62, −60	0.0014	0.3
Left cerebellum (6 & Crus 1)	−40, −52, −28	0.0044	0.2
Right putamen	28, 8, −12	0.0046	0.8
Left caudate nucleus	−12, 2, 8	0.0096	0.5
Right thalamus	8, −12, 2	0.0140	0.2

[a] FWE-corrected for multiple comparisons. Minimum *p* value derives from a permutation test with 5000 permutations. Extent refers to contiguous voxels below threshold *p* value. PCC, posterior cingulate cortex; (a/p)MCC, (anterior/posterior) midcingulate cortex; MTG, middle temporal gyrus; STG, superior temporal gyrus; ITG, inferior temporal gyrus; TPJ, temporo-parietal junction; MOG, middle occipital gyrus; DLPFC, dorsolateral prefrontal cortex; (a/p)VLPFC, (anterior/posterior) ventrolateral prefrontal cortex; STP, superior temporal pole; ACC, anterior cingulate cortex; MPFC, medial prefrontal cortex; (a/p)SFG, (anterior/posterior) superior frontal gyrus; SMA, supplementary motor area; MFG, middle frontal gyrus.

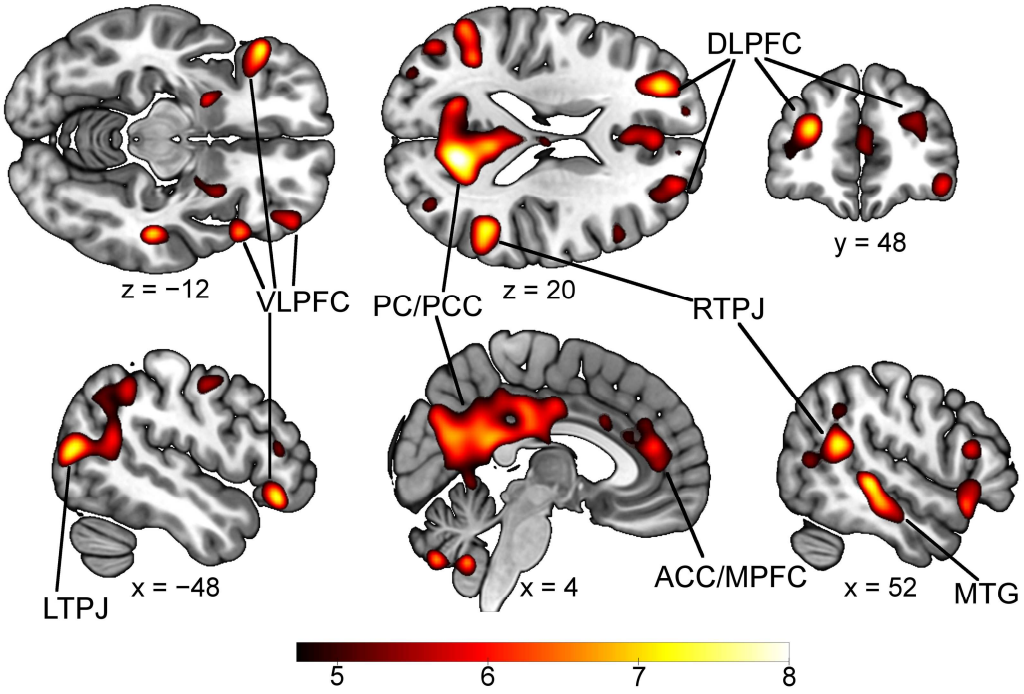

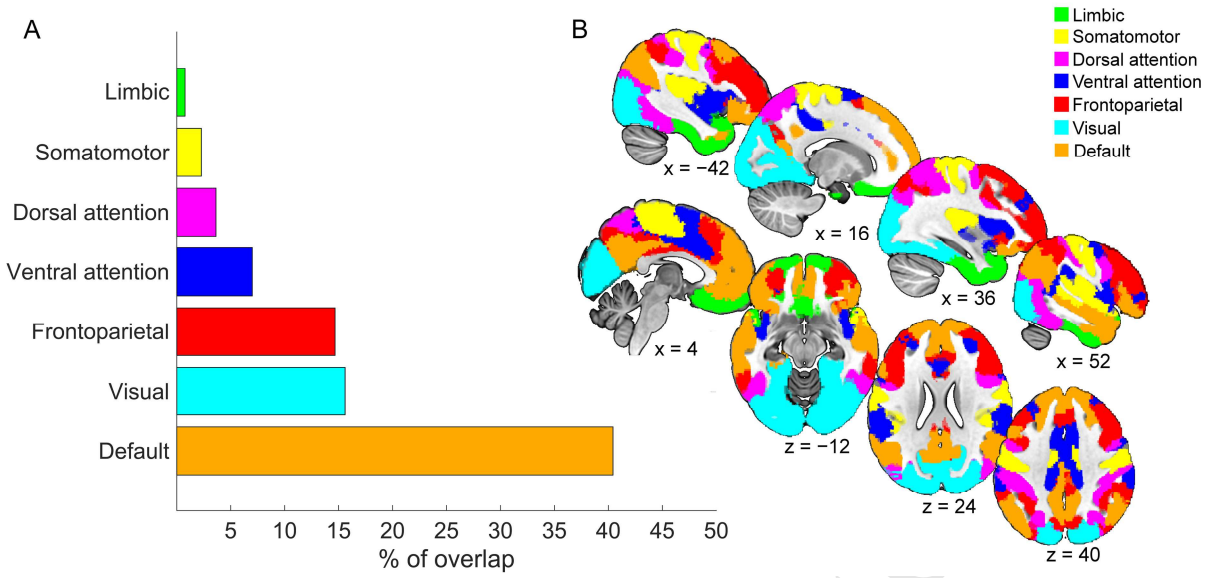

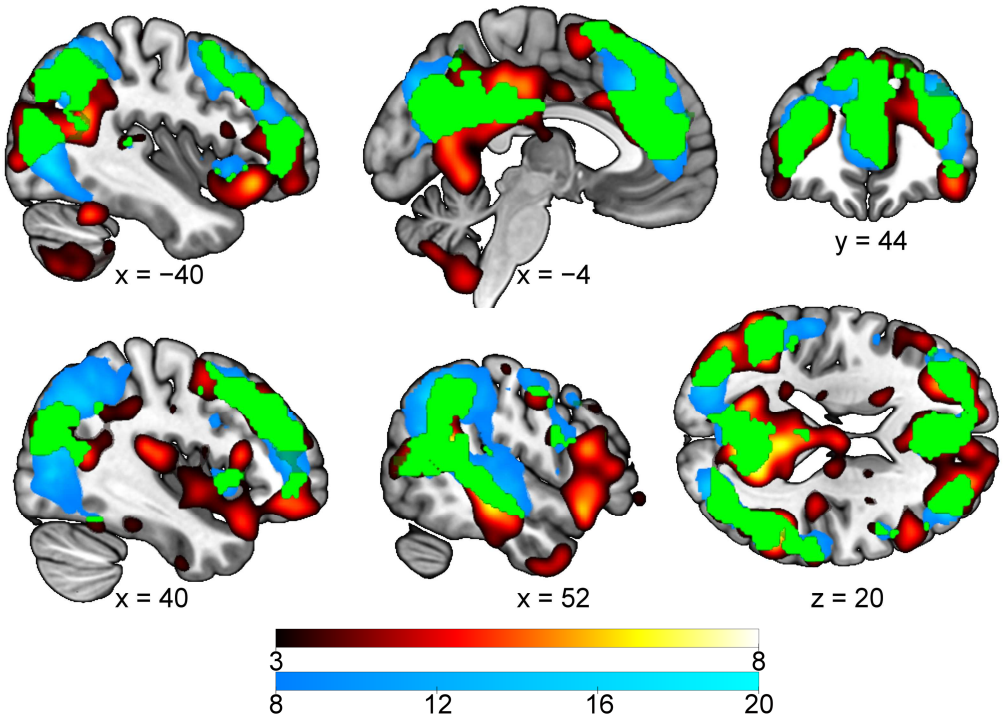

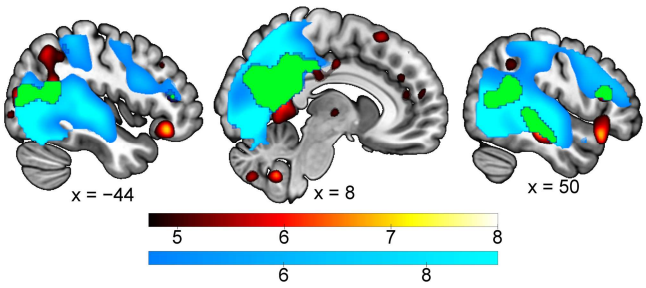

Aberrant Cortical Integration in First-Episode Psychosis During Natural Audiovisual Processing

Supplemental Information

Supplemental Methods

Extraction and statistical analyses of signal time courses from selected areas

To test whether there would be any specific time points in the movie that might contribute to the ISC differences, we extracted the BOLD signal eigenvariates from two masks: the areas of main task-related activity, that is, from visual and auditory areas shown in Figure S1, and from the network showing the most ISC differences between the groups. This latter mask is the intersection between the voxels where significant differences between the groups were found and the default-mode network (DMN), defined according to Yeo et al (1). We extracted the signals using DPABI V3.0 (2), and standardized them to z-scores using MATLAB R2014a. As ISC group difference may reflect difference in variance of signals in addition to difference in group mean, we also calculated a squared-difference from the group mean for each time point in each mask separately for each participant. Standardized signals and squared differences from the group mean were then compared between groups time-point-wise with a two-sample t test. P values were Bonferroni-corrected with 2 masks * 2 measures (z-scored and squared-difference signal) * 245 time points.

Supplemental Results

Supplemental results for confounding variables

Head movement

To confirm that the ISC group differences were not due to more head motion in the patient group, we divided the previously calculated ISC images from the patient group by the median framewise displacement value to high-motion (n = 26) and low-motion (n = 25) subgroups, the first including the one patient having the median value. Figures S2 and S3 show results from the comparison between the low- and high-motion groups vs the control subject group (primary $p < 0.001$, and FWE-corrected $p < 0.05$, $k \geq 421$ for the low-motion group and $k \geq 458$ for the high-motion group; a slightly more liberal threshold was applied here in order to show that the results are similarly spatially distributed in both subgroups as in the main analysis). In these models, the nuisance covariates are the same as in the main analysis, except for the mean framewise displacement. The results are broadly similar in both groups. Some clusters did not reach statistical significance in either subgroup separately as compared with the main analysis, as happened in right pVLPFC, left putamen and two of the cerebellar clusters for the low-motion subgroup and in left pre-/postcentral gyrus, superior medial frontal gyrus, left putamen, and three cerebellar clusters for the high-motion subgroup. However, it must be borne in mind that this analysis has markedly lower power than our primary analysis.

Attention

It could be argued that possible attentional differences are better controlled by regressing out ISC variability in the dorsal attention network (DAN) than the visual-auditory network used in the main analysis. To test whether this procedure would have any effects on the results, we extracted the eigenvariate values from DAN voxels, determined according to Yeo et al (1) and used them as a nuisance covariate in the general linear model in SnPM instead of the auditory and visual ISCs. Figure S4 and Table S2 show that results are comparable no matter how we control for the attentional confounds.

Data from two scanners

To verify that combining data from two scanners did not affect the results, we also separately analyzed data from the 37 patients and 21 control subjects scanned with the newer Siemens device; this was also the larger sub-sample. Figure S5 shows that most of the clusters present in the main group analysis were present in this subset (primary $p < 0.001$, FWE-corrected $p < 0.05$ at the cluster level, $k \geq 389$; a slightly more liberal threshold was applied here in order to show that the results are similarly spatially distributed in this subgroup as in the main analysis). However, some of these clusters were not present in the combined data from both scanners, which could indicate they are not robust across samples.

Could the ISC group differences be driven by few deviant individuals?

Given that within-group ISCs depend on all the other participants in the group, it is possible that one or few participants drive the group differences. In Figure S6 are shown the eigenvariate ISCs from the patient group across all the voxels that showed a significant difference in the main analysis. It can be seen that none of the patients showed highly deviant ISCs (all ISCs < 2*SD away from the mean) from these areas. Figure S7 shows the same thing from only those voxels of the significant group difference that coincide with the DMN (determined as in Yeo et al (1)); within these regions all ISCs < 2.65*SD away from the mean.

To compare with previous ISC studies, we report the differences in within-group ISCs as the main result. One way, in which the ISCs from the patients would be less susceptible to deviant activity in only few patients, is to calculate the ISC as the correlation of patient's voxel-wise time series to the same voxel in only the controls, that is, a patient-to-control ISC. We show in Figure S8 that such an analysis produces a very similar distribution of significant differences (primary $p < 0.001$, resulting in FWE-corrected $p < 0.05$ with $k \geq 379$). Thus, we find it unlikely that only one or few patients drive the reported main findings.

Supplemental Tables

Table S1. Mean ISCs from all the clusters that differed significantly between patients and control subjects.

Region	Control subjects (mean ISC)	Patients (mean ISC)
Bilateral precuneus, cuneus, PCC, pMCC, and calcarine cortex	0.0900	0.0461
Right MTG (incl. STG & ITG)	0.2477	0.1441
Left TPJ, incl. MOG	0.0990	0.0451
Right TPJ	0.1037	0.0445
Left calcarine and lingual gyri	0.0843	0.0447
Right posterior insula and Heschl's gyrus	0.0616	0.0228
Right fusiform gyrus	0.1074	0.0551
Right MOG	0.2066	0.1315
Left MOG	0.1172	0.0594
Left DLPFC	0.0498	0.0152
Left VLPFC, incl. STP	0.0465	0.0074
Right aVLPFC, incl. STP	0.0359	0.0090
Right pVLPFC	0.0585	0.0166
Bilateral ACC, aMCC and MPFC	0.0497	0.0174
Left pre- and postcentral gyrus	0.0886	0.0356
Right DLPFC	0.0684	0.0268
Right orbitofrontal cortex	0.0550	0.0184
Left aSFG and medial SFG	0.0697	0.0116
Right SMA and medial SFG	0.0636	0.0187
Left pSFG and medial SFG	0.0529	0.0191
Left SMA	0.0634	0.0210
Right (posterior) MFG and precentral gyrus	0.1092	0.0542
Left cerebellum (8)	0.0338	0.0094
Bilateral cerebellum (9 & Vermis 9)	0.0386	0.0163
Right cerebellum (7b, 8 & Vermis 8)	0.0518	0.0212
Right cerebellum (8 & 10)	0.0331	0.0017
Left putamen	0.0445	0.0120
Left cerebellum (Crus 2 & 7b)	0.1016	0.0410
Right cerebellum (8)	0.0436	0.0085
Left cerebellum (6 & Crus 1)	0.1904	0.0807
Right putamen	0.0326	0.0061
Left caudate nucleus	0.0378	0.0114
Right thalamus	0.0612	0.0224

PCC, posterior cingulate cortex; (a/p)MCC, (anterior/posterior) midcingulate cortex; MTG, middle temporal gyrus; STG, superior temporal gyrus; ITG, inferior temporal gyrus; TPJ, temporo-parietal junction; MOG, middle occipital gyrus; DLPFC, dorsolateral prefrontal cortex; (a/p)VLPFC, (anterior/posterior) ventrolateral prefrontal cortex; STP, superior temporal pole; ACC, anterior cingulate cortex; MPFC, medial prefrontal cortex; (a/p)SFG, (anterior/posterior) superior frontal gyrus; SMA, supplementary motor area; MFG, middle frontal gyrus.

Table S2. Group comparison of ISCs when controlling for the ISCs in the dorsal attention network. Table shows where ISCs are higher in control subjects.

Region	Peak (MNI) x, y, z	Minimum *p* value[a]	Extent (cm^3)
Bilateral precuneus, PCC, cuneus, pMCC, and calcarine gyrus	10, −64, 22	0.0002	14.256
Left DLPFC	−28, 46, 18	0.0002	1.816
Left VLPFC	−48, 32, −12	0.0002	1.952
Right MTG (incl. STG and ITG)	52, −30, −4	0.0002	2.088
Right TPJ	50, −48, 18	0.0002	2.384
Left MOG and pMTG	−48, −78, 12	0.0002	1.224
Right cerebellum (9)	6, −56, −46	0.0004	0.584
Right cerebellum (7b and Vermis 8)	4, −74, −44	0.0004	0.432
Left cerebellum (8)	−28, −62, −60	0.0004	0.216
Left TPJ	−58, −58, 20	0.0004	1.96
Right aVLPFC, incl. STP	48, 20, −16	0.0010	0.616
Right pVLPFC	46, 22, 14	0.0010	0.384
Bilateral aMCC	0, 16, 32	0.0038	0.176
Left pre- and postcentral gyrus	−52, −6, 46	0.0050	0.224
Right lingual gyrus	22, −56, 0	0.0050	0.224
Bilateral ACC	2, 42, 18	0.0068	0.704
Right Heschl's gyrus	40, −24, 14	0.0142	0.264
Right amygdala and putamen	24, 0, −10	0.0154	0.176

[a] FWE-corrected for multiple comparisons. Minimum *p* value derives from a permutation test with 5000 permutations. Extent refers to contiguous voxels below threshold *p* value.

Supplemental Figures

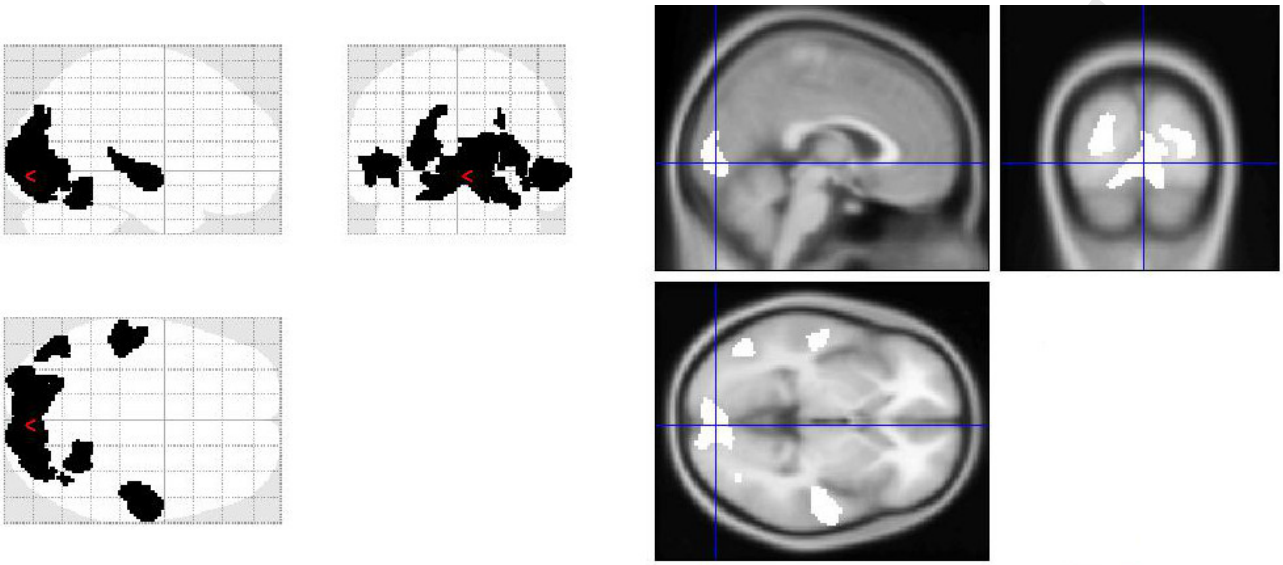

Figure S1. A mask was produced from a pooled sample of patients and control subjects (see the main text for details) including the regions with strongest (pseudo $t > 22$ used as a threshold) ISCs, that is, visual and auditory cortical areas.

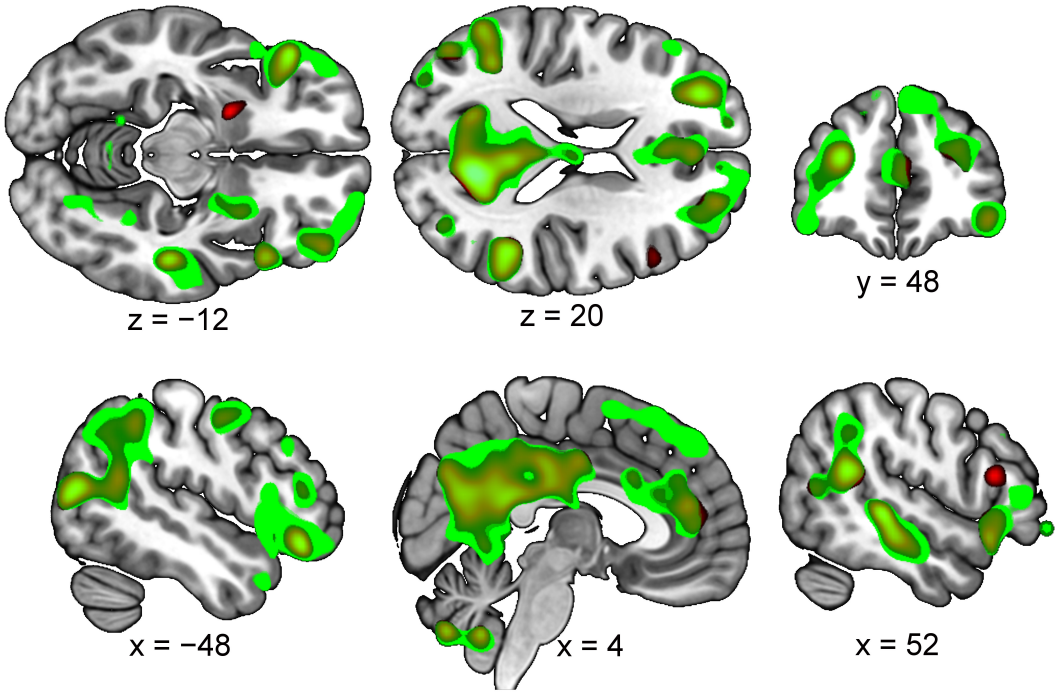

Figure S2. Low-motion subgroup (n = 25) compared to the control participants (n = 32). Figure shows areas where control participants had significantly higher ISCs (FWE-corrected $p < 0.05$ at cluster-level) in green. Overlaid in hot colors is the main group-level analysis from the main text. In the transversal slices, left hemisphere is up and in the coronal slice, left is left.

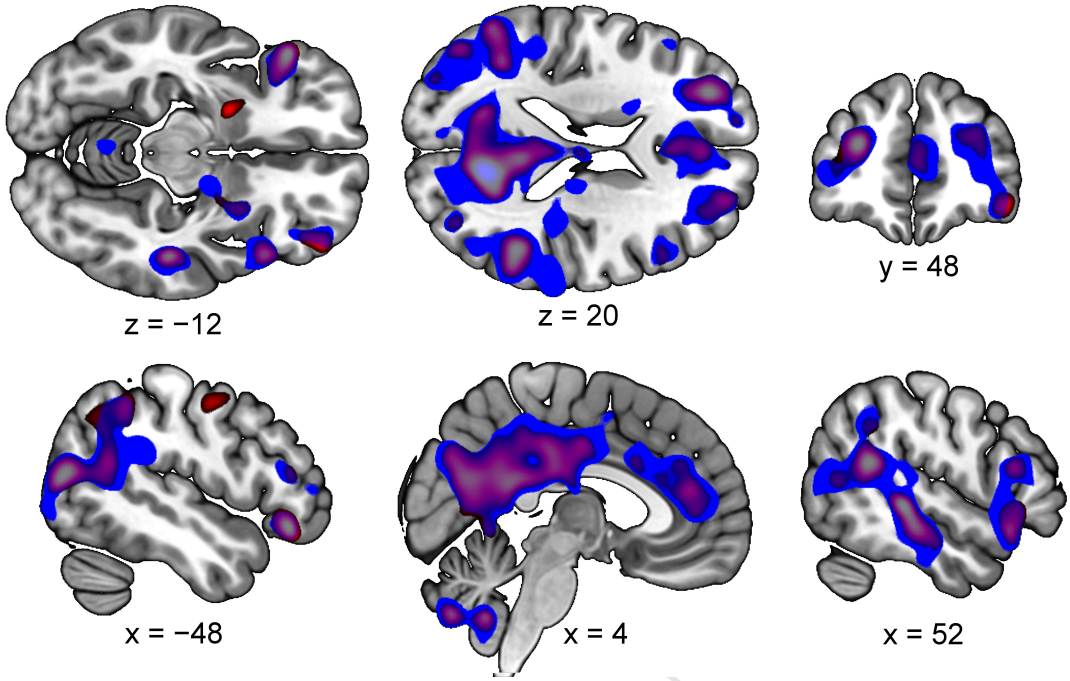

Figure S3. High-motion subgroup (n = 26) compared to the control participants (n = 32). Figure shows areas where control participants had significantly higher ISCs (FWE-corrected $p < 0.05$ at cluster-level) in blue. Overlaid in hot colors is the main group-level analysis from the main text. In the transversal slices, left hemisphere is up and in the coronal slice, left is left.

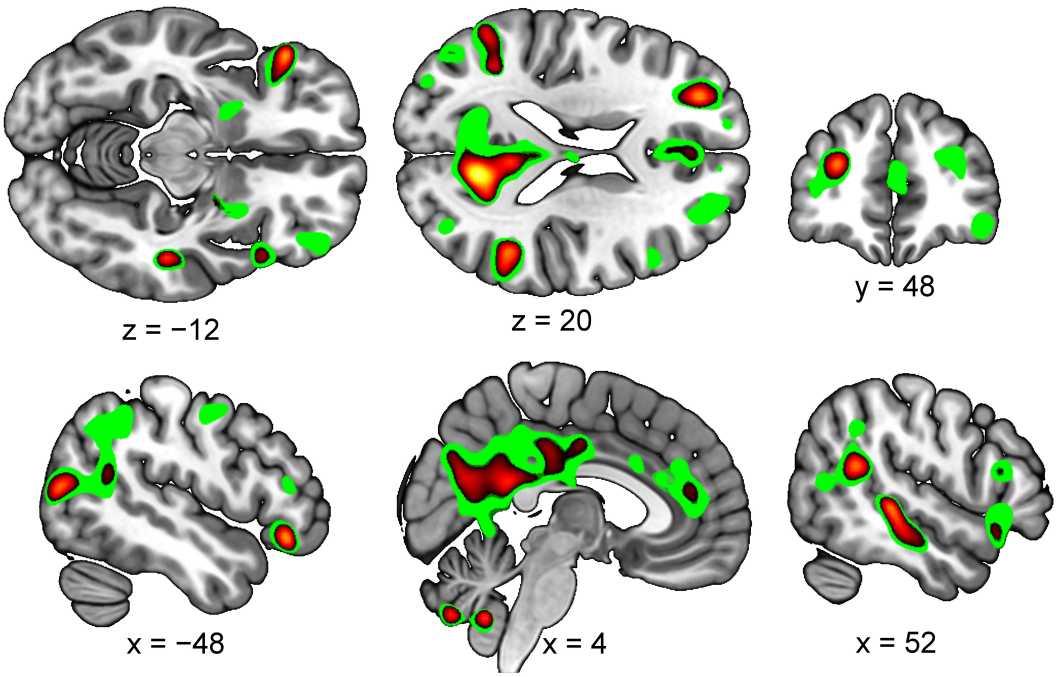

Figure S4. Figure shows dorsal attention network ISC-controlled group difference image in hot colors and the main reported ISC difference, that is, the auditory and visual ISC-controlled in green (both FWE-corrected voxel-wise $p < 0.05$, with at least 20 contiguous voxels). Areas where ISCs are higher in control participants are shown. In the transversal slices, left hemisphere is up and in the coronal slice, left is left.

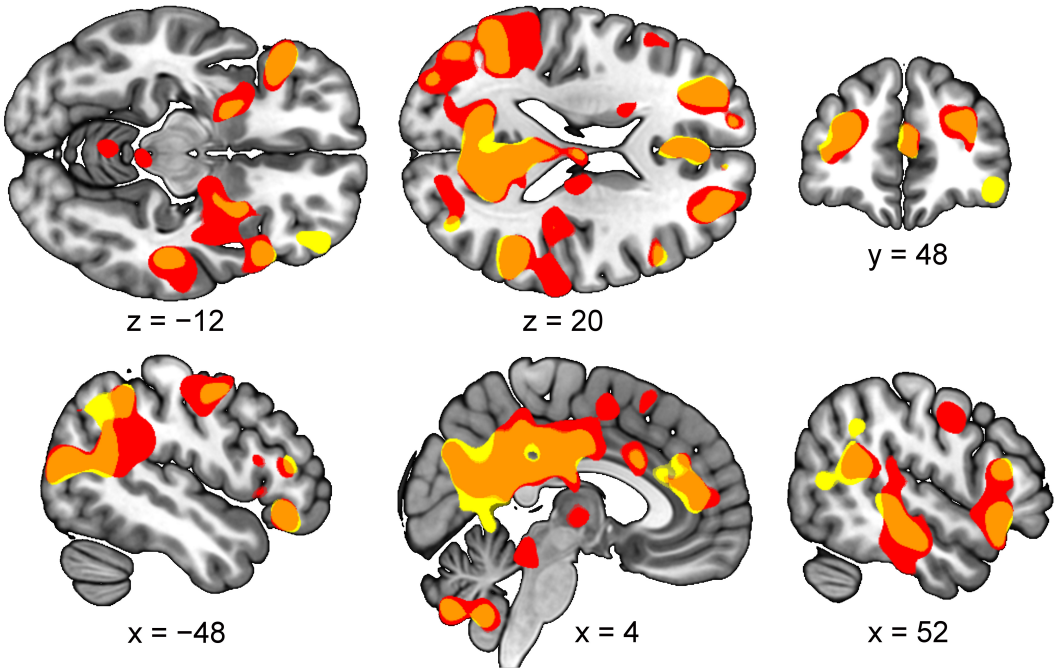

Figure S5. ISC group difference with the subsample whose data were acquired with the Siemens scanner. Figure shows regions where the control participants (n = 21) had higher ISCs than patients (n = 37) (cluster-level FWE-corrected p < 0.05) in the subsample whose data were acquired with the Siemens scanner (in red). The pooled data from the main analysis is shown in yellow, and the overlap between the two comparisons is shown in orange. In the transversal slices, left hemisphere is up and in the coronal slice, left is left.

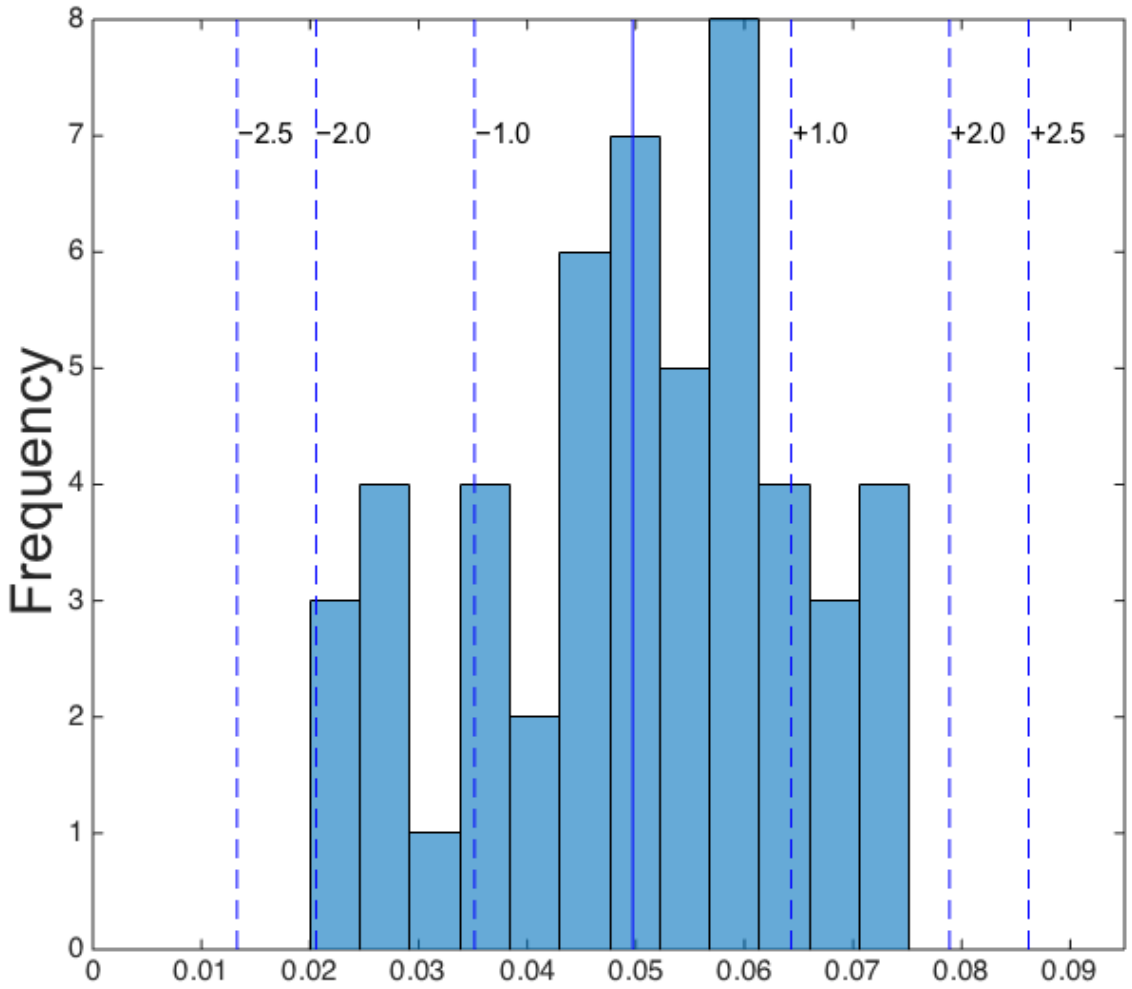

Figure S6. Distributions of patient ISC *r* eigenvariates extracted from a mask with all group differences. Mean = 0.05, indicated by the blue vertical line; SD = 0.015, SDs indicated by the blue dashed lines. No outliers are detected.

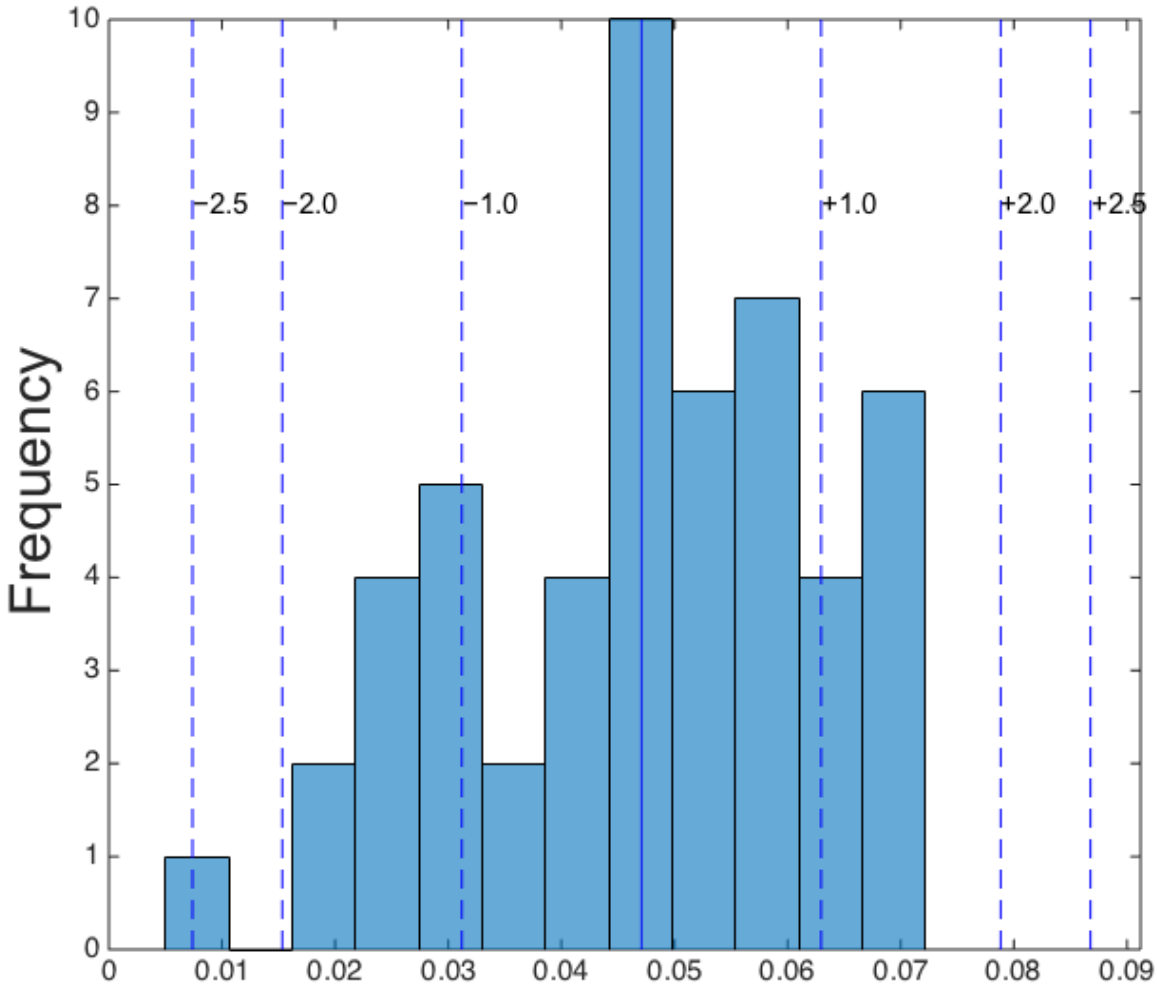

Figure S7. Distributions of ISC *r* eigenvariates extracted from voxels of the default-mode network (determined according to Yeo et al (1)) where the groups showed significant differences. Mean = 0.05, indicated by the blue vertical line; SD = 0.016, SDs indicated by the blue dashed lines. No outliers are detected.

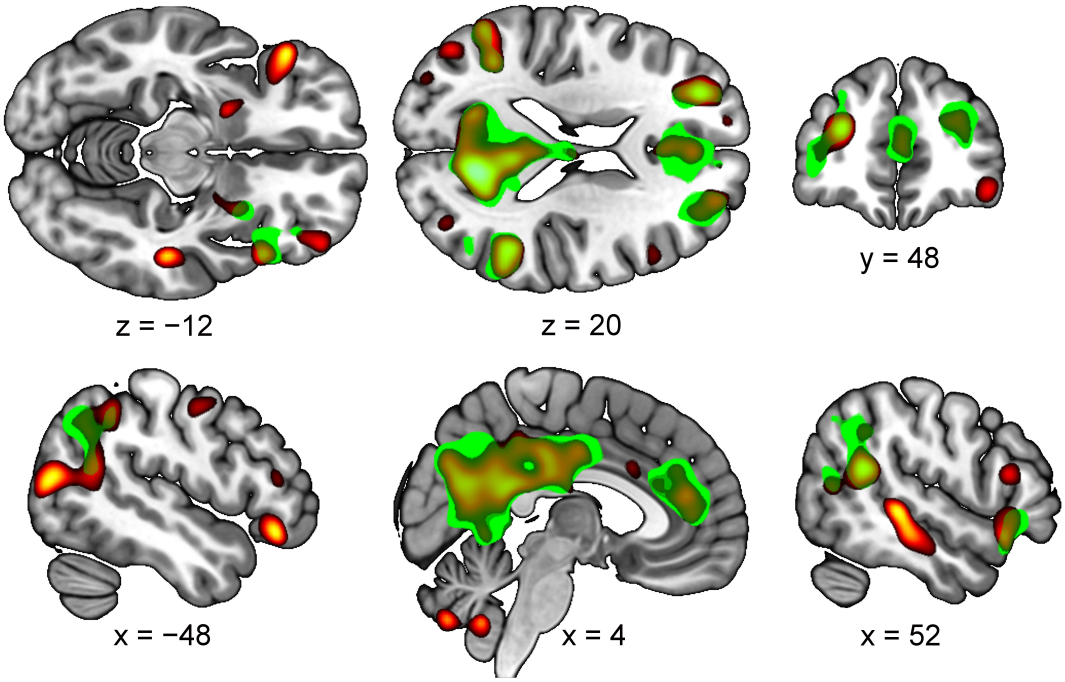

Figure S8. A control-to-control ISC vs patient-to-control ISC group comparison. Figure shows areas where control participants had significantly higher ISCs (FWE-corrected $p < 0.05$ at cluster-level) in green. The main group-level analysis from the main text is displayed in hot colors. In the transversal slices, left hemisphere is up and in the coronal slice, left is left.

Supplemental References

1. Yeo BTT, Krienen FM, Sepulcre J, Sabuncu MR, Lashkari D, Hollinshead M, et al (2011): The organization of the human cerebral cortex estimated by intrinsic functional connectivity. *J Neurophysiol* 106:1125–1165.

2. Yan C, Wang X, Zuo X, Zang Y (2016): DPABI: Data Processing & Analysis for (Resting-State) Brain Imaging. *Neuroinformatics* 14:339–351.